Research Square

Preprints are preliminary reports that have not undergone peer review.
They should not be considered conclusive, used to inform clinical practice,
or referenced by the media as validated information.

Ptpn20 maintains choroid plexus epithelial integrity to preserve amyloid-β homeostasis in Alzheimer's disease

Ryo Miyahara
Juntendo University Graduate School of Medicine
Masakazu Miyajima
mmasaka@juntendo.ac.jp

Juntendo University Graduate School of Medicine
Madoka Nakajima
Juntendo University Graduate School of Medicine
Ikuko Ogino
Juntendo University Graduate School of Medicine
Ko Horikoshi
Juntendo University Graduate School of Medicine
Koichiro Sakamoto
Juntendo University Graduate School of Medicine
Kaito Kawamura
Juntendo University Graduate School of Medicine
Chihiro Akiba
Juntendo University Graduate School of Medicine
Shinya Yamada
Juntendo University Graduate School of Medicine
Kostadin Karagiozov
Juntendo University Graduate School of Medicine
Chihiro Kamohara
Juntendo University Graduate School of Medicine
Eri Nakamura
Juntendo University Graduate School of Medicine
Nobuhiro Tada
Juntendo University Graduate School of Medicine
Akihide Kondo
Juntendo University Graduate School of Medicine

Research Article

Keywords: Choroid plexus, Blood–CSF barrier, Amyloid-β homeostasis, Alzheimer's disease, Ptpn20, RhoA signaling, Epithelial integrity, Vesicle-associated transport

Posted Date: August 25th, 2026

DOI: https://doi.org/10.21203/rs.3.rs-10596838/v1

License: This work is licensed under a Creative Commons Attribution 4.0 International License. Read Full License

Additional Declarations: No competing interests reported.

Abstract

Background: The choroid plexus forms the blood–cerebrospinal fluid (CSF) barrier and plays a central role in brain homeostasis through CSF production and solute exchange. Although age-related choroid plexus dysfunction has been implicated in Alzheimer's disease (AD), the molecular mechanisms that preserve epithelial integrity and amyloid-β homeostasis remain poorly understood.

Methods: To investigate the role of the cytoplasmic protein tyrosine phosphatase Ptpn20 in maintaining choroid plexus epithelial integrity, we analyzed Ptpn20-deficient mice and amyloid precursor protein (APP) knock-in mice using transcriptomic profiling, immunohistochemistry, RhoA activity assays, electron microscopy, biochemical analyses, and behavioral testing.

Results: Loss of Ptpn20 disrupted apical F-actin organization and epithelial architecture in the choroid plexus. In APP knock-in mice, Ptpn20 deficiency promoted persistent ventricular-facing retention of amyloid-β despite largely preserved expression of major transport-related genes. These changes were accompanied by coordinated alterations in epithelial transport- and vesicle-associated pathways, early epithelial junctional abnormalities, progressive loss of apical microvilli and cilia, mitochondrial abnormalities, and marked reduction of apical vesicle-like structures. Choroid plexus epithelial dysfunction was further associated with accelerated cerebral amyloid deposition, synaptic degeneration, and cognitive impairment.

Conclusions: Ptpn20 is a key regulator of choroid plexus epithelial integrity required for maintaining blood–CSF barrier homeostasis and physiological amyloid-β homeostasis. These findings identify choroid plexus epithelial dysfunction as a previously underrecognized mechanism promoting Alzheimer's disease pathology.

Introduction

Alzheimer’s disease (AD) is characterized by progressive accumulation of amyloid-β (Aβ), reflecting an imbalance between its production and clearance rather than overproduction alone [1-6]. While impaired clearance has emerged as a central driver of early AD pathogenesis, the mechanisms governing Aβ movement across cerebrospinal fluid (CSF) interfaces remain incompletely understood. The choroid plexus (ChP), a highly vascularized epithelial structure forming the blood–CSF barrier, plays a pivotal role in CSF production and turnover, as well as the removal of metabolic waste from the central nervous system [7-11]. ChP epithelial cells possess a dense apical F-actin network that stabilizes tight junctions, maintains microvillar architecture, and is associated with receptor-mediated endocytic processes [12-14]. These actin-dependent epithelial structures are increasingly recognized as important regulators of receptor-mediated uptake, membrane trafficking, and amyloid-β homeostasis at the blood–CSF barrier[15-17].

Structural deterioration of the ChP epithelium—including disruption of apical F-actin, microvillar atrophy, and impaired vesicle-associated transport organization—has been reported during aging and in

neurological disorders associated with disturbed CSF homeostasis [15-17]. These abnormalities have been associated with reduced CSF production, impaired metabolite clearance, and diminished epithelial transport capacity, thereby compromising amyloid-β handling. Similar epithelial alterations have also been reported in disorders characterized by impaired CSF dynamics, including idiopathic normal pressure hydrocephalus [18-21]. However, the molecular mechanisms responsible for maintaining epithelial architecture and transport competence remain poorly understood.

Protein tyrosine phosphatases (PTPs) regulate epithelial architecture through modulation of cytoskeletal dynamics, cell adhesion, and Rho-family GTPase signaling [22-25]. Among this family, Ptpn20 remains one of the least characterized members, although available evidence suggests that it participates in actin remodeling and RhoA signaling [22, 23]. Based on these observations, we hypothesized that Ptpn20 maintains apical epithelial integrity required for membrane organization and physiological amyloid-β homeostasis.

Here, we combined transcriptomic, ultrastructural, biochemical, and genetic analyses to define the role of Ptpn20 in ChP epithelial homeostasis. Using Ptpn20-deficient mice and APPNL-G-F knock-in mice [26], we demonstrate that loss of Ptpn20 disrupts apical actin organization, promotes progressive epithelial degeneration, and results in persistent ventricular-facing retention of Aβ within the choroid plexus. Together, these findings identify Ptpn20 as a previously unrecognized regulator of choroid plexus epithelial integrity that preserves amyloid-β homeostasis at the blood–CSF barrier, establishing the choroid plexus as an important determinant of Alzheimer's disease pathogenesis.

Materials and Methods

Animals

All experimental animals were group-housed (2–5 mice per cage) in a temperature- and humidity-controlled facility (23 ± 1 °C, 55 ± 5% humidity) under a 12-h light/12-h dark cycle at the Center for Experimental Medicine, Juntendo University, Japan. All animal procedures were approved by the Ethics Review Committee for Animal Experimentation of the Juntendo University School of Medicine (approval no. 1337) and were conducted in accordance with the National Institutes of Health guidelines for the care and use of laboratory animals. Animals were monitored daily for health status, and no unexpected adverse events were observed.

Only male mice were used in this study. Mice were deeply anesthetized with a mixed anesthetic agent (medetomidine 0.3 mg/kg, midazolam 4.0 mg/kg, and butorphanol 5.0 mg/kg; intraperitoneal injection) and euthanized by decapitation. Brain tissues were rapidly dissected and processed as described below. Sample sizes were determined based on previous studies and our prior experience with these experimental paradigms.

Mouse lines

C57BL/6J mice were used as wild-type (WT) controls. Ptpn20 knockout mice (Ptpn20$^{-/-}$; hereafter referred to as Ptpn20KO) were generated using CRISPR/Cas9 technology as previously described (Xu et al., 2022). App^NL-G-F/NL-G-F knock-in mice (RBRC06344; hereafter referred to as APPKI) were obtained from RIKEN BioResource Center and maintained on a C57BL/6J background. These mice harbor three familial Alzheimer's disease mutations (Swedish, Iberian, and Arctic) introduced into the endogenous App locus. Double-mutant APPKI × Ptpn20KO mice were generated by crossing homozygous APPKI mice with homozygous Ptpn20KO mice (Fig. S2).

Genotyping

Genomic DNA was extracted from tail biopsies, and genotyping was performed by PCR using the following primers (Table 1).

Microarray analysis

Choroid plexuses were isolated from 4-week-old WT and Ptpn20KO mice. Total RNA was extracted using the RNeasy Mini Kit (Qiagen) from RNAlater-stabilized tissue. RNA quality was assessed using a 4150 TapeStation (Agilent). Gene expression profiling was performed using the GeneChip Mouse Exon 1.0 ST Array (Affymetrix), and data were normalized using the Robust Multichip Average algorithm. Differentially expressed genes were analyzed using Transcriptome Analysis Console software and Ingenuity Pathway Analysis. Differentially expressed genes were defined using a $\log_2$ fold-change threshold of ±0.5 combined with moderated t-statistics and Benjamini–Hochberg false discovery rate correction. Functional module scores were calculated as the mean signed $\log_2$ fold change of genes assigned to each predefined module. Visualization was performed using R and Prism.

Quantitative reverse transcription PCR (RT-qPCR)

Total RNA (500 ng) was reverse-transcribed using SuperScript IV VILO Master Mix. RT-qPCR was performed using TaqMan Gene Expression Assays on an ABI 7500 system. Gene expression levels were normalized to Actb, and all reactions were performed in triplicate. (Table 2)

Immunofluorescence

Brains were fixed in 4% paraformaldehyde, embedded in paraffin or cryoprotected, and sectioned. In addition, choroid plexus tissue was processed using a paraformaldehyde-fixed whole-mount (free-floating) immunofluorescence staining protocol. Sections were blocked and incubated with primary antibodies overnight at 4 °C, followed by appropriate secondary antibodies. Nuclei were counterstained with DAPI. Images were acquired using a Leica TCS-SP5 confocal microscope. (Table 3, 4)

Protein expression of Ptpn20

Proteins were extracted from ChP tissue and lysed in 50 µl of lysis buffer (N-PER; Thermo Fisher Scientific, Waltham, MA, USA) containing a protease inhibitor cocktail (cOmplete ULTRA Mini EDTA-free

EASYpack; Roche, Basel, Switzerland). Lysates were clarified by centrifugation at 20,000 × g for 10 min at 4 °C, and protein concentrations in the supernatants were determined using a BCA Protein Assay Kit (Thermo Fisher Scientific). Protein samples (10–15 µg) were mixed with NuPAGE® LDS Sample Buffer (NP0008; Invitrogen) and NuPAGE® Sample Reducing Agent (NP0009; Invitrogen), heated at 70 °C for 10 min, and separated on 4–12% NuPAGE® Bis-Tris Mini Gels using NuPAGE® MOPS SDS Running Buffer (NP0001; Invitrogen). Proteins were then transferred onto polyvinylidene fluoride membranes. Membranes were incubated with rabbit anti-PTPN20B antibody (CSB-PA065165; CusAb; 1:500 dilution). Immunoreactive signals were detected by chemiluminescence using a WesternBreeze kit (WB7103; Invitrogen). Bands were visualized and analyzed using Image Lab software version 4.1 (Bio-Rad Laboratories, Hercules, CA, USA). The same antibody was used for both immunofluorescence and western blot analyses.

Cisterna magna injection of Carbon Black

Eight-week-old Ptpn20KO mice were anesthetized and placed in a stereotaxic frame. A total of 10 µl of 1% Carbon Black suspension was slowly injected into the cisterna magna using a 29-gauge microsyringe. Mice were maintained in a head-down position for 5 min. Thirty minutes after injection, mice were perfused with PBS followed by 4% paraformaldehyde.

Immunohistochemistry and plaque quantification

Paraffin sections were stained with anti-Aβ antibody (82E1) and visualized using DAB. Plaque burden was expressed as the percentage of 82E1-positive area within predefined cortical and hippocampal ROIs using Fiji software (NIH). Data acquisition and quantitative analyses were performed by investigators blinded to genotype whenever feasible. (Table 4)

Electron microscopy

Choroid plexus tissues were fixed with paraformaldehyde and glutaraldehyde, postfixed with osmium tetroxide, dehydrated, and embedded for transmission electron microscopy (TEM) or processed for scanning electron microscopy (SEM) according to standard protocols.

Ultrastructural quantification of apical vesicle-like structures

To quantify apical vesicle-like structures, ultrastructural analysis was performed using transmission electron micrographs. Apical membrane length was traced and measured using Fiji software (NIH). Membrane-bound vesicle-like structures measuring 50–150 nm in diameter and located within 2 µm of the apical membrane were counted in a blinded manner. Vesicle density was expressed as the number of vesicle-like structures per μm^2 of apical epithelial area. Analyses were performed using randomly selected epithelial regions from multiple independent animals.

RhoA activity assay

Active RhoA and total RhoA were measured independently using G-LISA and ELISA assays, respectively. The active-to-total RhoA ratio was subsequently calculated.

ELISA

Aβ40 and Aβ42 levels in ChP homogenates were quantified using Human/Rat βAmyloid(40)ELISA Kit Wako and Human/Rat βAmyloid(42)ELISA Kit Wako, High-Sensitive (FUJIFILM Wako Pure Chemical Corporation, Osaka, Japan). Quantification was performed by an investigator blinded to genotype.

Behavioral assessment

Behavioral analyses were performed using the Y-maze and Morris water maze. To test spatial memory, we conducted the Y-maze test with 24- and 48-week-old mice, using the same subjects for both trials. The apparatus consisted of three 30 cm × 7 cm arms. Mice were placed at the end of one arm and allowed to explore for 8 minutes. Tracks were recorded using a Y-maze Video Tracking System (Muromachi Kikai, Tokyo, Japan). Percent alternation, defined as consecutive entries into three different arms divided by total entries minus 2, was calculated. An entry was defined as traveling at least 4 cm into an arm.

For spatial memory and learning, we performed the Morris Water Maze with the same mice. The apparatus was a blue circular pool (65 cm diameter) with opaque water and a submerged escape platform (7.5 cm diameter) positioned in one of four quadrants. Water temperature was maintained at 19 ± 2°C. Four visual cues were placed on the pool wall. During the learning periods, the platform was submerged in Q1, and mice were placed at the center of the pool. Mice were trained to find and climb the hidden platform. Each trial lasted 60 seconds, during which the mice sought the platform, and upon finding it, they remained on it for 10 seconds. If unsuccessful, the mice were guided to the platform and allowed to stay for 10 seconds. Latency to find the platform and swim paths were recorded using the Morris Water Maze 9Video Tracking System. Three trials per day were conducted. On the 10th day, during the probe test, the platform was removed, and mice swam freely for 90 seconds. Time spent in Q1 and swim paths were recorded. This study was designed and reported in accordance with the ARRIVE 2.0 guidelines.

Statistics

Primary outcome measures included Aβ accumulation, choroid plexus structural integrity, and behavioral performance. Statistical analyses were performed using IBM SPSS Statistics v29. Appropriate statistical tests are described in the figure legends. A two-sided P value < 0.05 was considered statistically significant. Data are presented as mean ± s.e.m. or mean ± s.d., as indicated in the figure legends. Animals were assigned to experimental groups according to genotype and age and were housed under identical conditions without systematic allocation bias. Investigators were blinded to genotype during image acquisition and quantitative analyses whenever feasible.

The conceptual illustration shown in Fig. 6 was generated with the assistance of artificial intelligence-based image generation tools and subsequently modified and curated by the author.

Results

Ptpn20 deficiency disrupts ChP epithelial integrity

In 8-week-old wild-type (WT) mice, Ptpn20 immunoreactivity was diffusely detected in the cytoplasm of ChP epithelial cells, whereas no Ptpn20 immunoreactivity was observed in Ptpn20 knockout (Ptpn20KO) mice. Loss of Ptpn20 was accompanied by marked disruption and attenuation of the apical F-actin network, indicating impaired epithelial cytoskeletal organization (Fig. 1a). Western blot analysis confirmed the absence of Ptpn20 protein expression in Ptpn20KO ChP tissue (Fig. 1b). AQP1 immunoreactivity in WT ChP epithelium was predominantly localized along the apical membrane, whereas Ptpn20KO mice exhibited a less continuous and more irregular staining pattern with partial redistribution toward the cytoplasmic compartment, consistent with altered apical membrane organization (Fig. 1c).

Claudin-1 immunoreactivity was markedly reduced in Ptpn20KO ChP epithelium, consistent with impaired epithelial junctional integrity (Fig. 1d). RhoA immunoreactivity was detected along the apical epithelial membrane in both WT and Ptpn20KO mice at 8 weeks of age (Fig. 1e). By 16 weeks, apical F-actin organization appeared further disrupted in Ptpn20KO mice, consistent with progressive deterioration of epithelial cytoskeletal organization (Fig. 1f).

Tracer retention suggests altered epithelial handling of ventricular solutes in Ptpn20-deficient ChP

To assess the functional consequences of epithelial structural abnormalities, we examined tracer distribution following intracisternal Carbon Black injection. WT mice exhibited minimal tracer retention along the ChP epithelium, whereas Ptpn20KO mice showed prominent retention at the apical epithelial surface (Fig. 1g). Although this approach does not directly quantify specific endocytic or transcytotic pathways, the observed apical tracer retention is consistent with altered apical membrane dynamics and handling of ventricular particulate contents in Ptpn20-deficient ChP.

Ptpn20 deficiency disrupts epithelial transport and cytoskeletal gene networks associated with Aβ handling

Microarray analysis of ChP tissue from 4-week-old WT and Ptpn20KO mice was organized into eight predefined functional gene modules: (1) uptake/transcytosis, (2) efflux transport, (3) degradation, (4) CSF/ion dynamics, (5) barrier/inflammation, (6) metal homeostasis, (7) stress/mTOR signaling, and (8) cytoskeleton/vesicle-associated transport organization. Heat map analyses revealed coordinated alterations across multiple functional gene modules in Ptpn20KO mice, the greatest coordinated alterations were observed in uptake/transcytosis, degradation, barrier/inflammation, and cytoskeleton/vesicle-associated transport organization pathways (Fig. 2a, Table S1). RT–qPCR at 5

weeks confirmed significant reductions in Cav1 and Cltc, genes associated with caveolae- and clathrin-mediated endocytic processes, respectively (Fig. 2b). Expression of Abcc1, a transporter implicated in basolateral efflux at the choroid plexus, was significantly reduced, whereas Lrp1 expression remained unchanged. Aqp1 expression was also significantly downregulated, while Atp1a1 and Slc13a3 showed no significant changes. Collectively, these findings indicate that loss of Ptpn20 is associated with coordinated alterations in epithelial transport, vesicle-associated trafficking, and cytoskeletal organization within the ChP epithelium.

Altered RhoA signaling dynamics in Ptpn20-deficient ChP

Because RhoA is a central regulator of actin polymerization and membrane-associated cytoskeletal dynamics, we quantified its activation state using G-LISA and ELISA assays. At 5–6 weeks of age, levels of active, GTP-bound RhoA were significantly elevated in Ptpn20KO ChP compared with WT controls (WT: 0.087 ± 0.012; KO: 0.184 ± 0.014; $p = 0.001$). In contrast, this genotype-dependent difference was no longer detectable at 8 weeks (WT: 0.138 ± 0.031; KO: 0.151 ± 0.012) (Fig. 2c). Total RhoA protein levels were modestly but significantly increased in Ptpn20KO mice at both 5–6 weeks and 8 weeks ($p < 0.05$ for both comparisons) (Fig. 2d). Accordingly, the ratio of active to total RhoA—a measure of the fraction of RhoA in its GTP-bound state—was significantly elevated in Ptpn20KO mice at 5–6 weeks (WT: 3.46 ± 0.66; KO: 5.73 ± 0.58; $p = 0.049$), but not at 8 weeks (WT: 6.31 ± 1.35; KO: 5.94 ± 0.49) (Fig. 2e). Together, these findings suggest that loss of Ptpn20 is associated with an early, transient increase in RhoA activation, followed by a return toward WT levels despite persistent alterations in apical actin organization. These findings indicate dynamic changes in RhoA signaling associated with persistent epithelial cytoskeletal abnormalities.

Ptpn20 deficiency promotes persistent ventricular-facing amyloid-β retention in the choroid plexus of APPKI mice

Genotyping confirmed successful generation of APPKI × Ptpn20KO double-mutant mice (Fig. S2). Immunofluorescence analysis revealed marked accumulation of Aβ along the ventricular-facing apical surface of the ChP epithelium in APPKI×Ptpn20KO mice compared with APPKI mice. In APPKI mice, only minimal Aβ immunoreactivity was observed, whereas APPKI×Ptpn20KO mice exhibited prominent apical Aβ retention along the ventricular-facing epithelial surface of the ChP. These findings indicate that Ptpn20 deficiency is associated with abnormal apical retention of Aβ at the ChP epithelium (Fig. 3a). ELISA quantification of whole ChP tissue lysates—which reflects both intracellular Aβ and Aβ molecules bound or retained at the apical epithelial surface—revealed significantly elevated levels of both Aβ40 and Aβ42 in APPKI × Ptpn20KO mice compared with APPKI controls (Fig. 3b). At 16 weeks of age, double immunofluorescence analysis demonstrated persistent differences in the spatial distribution of amyloid-β within the choroid plexus. In APPKI mice, mild amyloid-β immunoreactivity was observed predominantly within the stromal region, whereas APPKI×Ptpn20KO mice exhibited prominent amyloid-β deposition along the ventricular-facing epithelial surface (Fig. 3c).

At 7 weeks of age, RT–qPCR analysis demonstrated selective alterations in epithelial transport-related gene expression in APPKI×Ptpn20KO mice (Fig. 3d). Among the genes examined, Aqp1 and Slc13a3 expression levels were increased compared with APPKI controls, whereas expression of Lrp1, Atp1a1, Abcc1, Cav1, and Cltc remained largely unchanged. Notably, despite the absence of significant changes in Lrp1 mRNA expression, APPKI×Ptpn20KO mice exhibited persistent ventricular-facing amyloid-β retention, suggesting that impaired epithelial Aβ handling may not be explained solely by altered expression of known transport-related genes.

Ultrastructural analysis at 8 weeks of age demonstrated relatively preserved overall epithelial architecture in APPKI mice, whereas APPKI×Ptpn20KO mice exhibited abnormalities at the apical junctional region together with enlarged intercellular spaces, indicating early disruption of epithelial integrity (Fig. 4a). By 16 weeks of age, epithelial abnormalities had progressed substantially in APPKI×Ptpn20KO mice, with altered cytoplasmic organization, marked loss of apical microvilli and cilia, and disruption of the apical epithelial surface, as demonstrated by TEM and SEM analyses (Fig. 4b,c). In addition, mitochondrial profiles appeared irregular compared with APPKI controls.

Ultrastructural quantification further demonstrated a marked reduction in apical vesicle-like structures in choroid plexus epithelial cells of APPKI×Ptpn20KO mice compared with APPKI mice. The mean density of apical vesicle-like structures was 0.44 ± 0.02/μm² in APPKI mice and 0.15 ± 0.01/μm² in APPKI×Ptpn20KO mice ($p < 0.001$) (Fig. 4d). These findings indicate substantial alterations in the organization of apical vesicle-like structures in Ptpn20-deficient ChP epithelium.

Combined Ptpn20 deficiency and amyloid pathology accelerates brain Aβ deposition, synaptic degeneration, and cognitive impairment

At 8 weeks of age, amyloid plaque burden was significantly increased in the cerebral cortex of APPKI × Ptpn20KO mice compared with APPKI mice (Fig. 5a,b). By 16 weeks, plaque deposition had increased substantially in both genotypes, but remained significantly greater in APPKI×Ptpn20KO mice in both cortex and hippocampus (Fig. 5c,d). Transmission electron microscopy of the hippocampal CA3 region revealed a significant reduction in synaptic structures in APPKI × Ptpn20KO mice relative to APPKI controls (Fig. 5e,f).

Behavioral analyses at 24 weeks demonstrated significant cognitive impairment in APPKI×Ptpn20KO mice. In the Y-maze, spontaneous alternation rates were significantly reduced compared with APPKI mice, indicating impaired working memory (Fig. 5g). Ptpn20KO mice without APPKI did not exhibit significant impairment, indicating that cognitive deficits became most apparent in the presence of amyloid pathology. In the Morris water maze, APPKI×Ptpn20KO mice exhibited impaired acquisition performance and reduced spatial memory retention, as reflected by decreased target-zone crossings during the probe test (Fig. S3a–c). Together, these findings indicate that loss of Ptpn20 exacerbates amyloid-associated neuropathology and cognitive impairment.

Discussion

The choroid plexus (ChP) is increasingly recognized as a dynamic regulatory interface that contributes to cerebrospinal fluid (CSF) turnover, molecular exchange, and metabolic homeostasis within the central nervous system [7, 8, 12]. Specialized ChP epithelial cells contain a dense apical F-actin network that supports tight junction integrity, microvillar morphology, and receptor-mediated endocytic processes [12-17], thereby contributing to coordinated handling of metabolites, including Aβ and other neurotoxic species at the CSF–blood interface. Age-related deterioration of these cytoskeletal structures has been linked to reduced CSF production and impaired clearance of Aβ [15-17]; however, the molecular mechanisms that preserve epithelial integrity and vesicle-associated transport organization remain poorly defined.

In this study, we identify the cytoplasmic non-receptor protein tyrosine phosphatase Ptpn20 as an important regulator of actin-associated epithelial organization in ChP epithelial cells. Loss of Ptpn20 destabilized apical F-actin architecture, disrupted microvillar organization, and was associated with altered expression of genes related to caveolae- and clathrin-mediated endocytic processes. These structural and molecular alterations were accompanied by coordinated transcriptional downregulation of cytoskeletal, junctional, and vesicle-associated transport modules, yielding a molecular signature that resembles aged or metabolically compromised ChP tissue [15-17]. Together, these findings support a role for Ptpn20 in maintaining choroid plexus epithelial integrity through preservation of apical epithelial organization and vesicle-associated transport.

A key mechanistic observation from our work is the biphasic alteration of RhoA signaling associated with Ptpn20 deficiency. RhoA is a central regulator of actin polymerization, membrane dynamics, and cytoskeletal organization, processes closely linked to epithelial membrane organization [27-29]. Using quantitative G-LISA and ELISA assays, we observed an early, transient increase in RhoA activation at 5–6 weeks of age, reflected by increased levels of GTP-bound RhoA and an elevated active-to-total RhoA ratio. This increase was no longer apparent by 8 weeks, despite persistently elevated total RhoA expression. We interpret this temporal pattern not as normalization of cytoskeletal regulation, but rather as progressive alteration in the coordination between RhoA signaling and the apical actin scaffold as epithelial structural integrity deteriorates. Such spatial and functional uncoupling may reflect a transition from an early compensatory response toward dysregulated cytoskeletal signaling insufficient to maintain normal epithelial architecture. Specifically, early transient hyperactivation of RhoA may disturb normal actin dynamics, ultimately leading to failure of maintaining a functional apical F-actin network.

The Carbon Black tracer experiments further support this interpretation by demonstrating abnormal retention of an apically encountered particulate tracer, providing supportive evidence that loss of apical F-actin disrupts membrane-associated handling dynamics at the ventricular surface, prior to overt microvillar degeneration.

The functional consequences of Ptpn20-dependent cytoskeletal dysregulation became particularly evident under Aβ-associated stress conditions. The APP^NL-G-F background enabled us to evaluate the consequences of epithelial dysfunction under conditions of chronic amyloid stress [26]. In the APP^NL-

G-F knock-in background, combined loss of Ptpn20 produced a severe epithelial phenotype characterized by pronounced apical Aβ retention, disruption of claudin-1 continuity, severe loss of microvilli and cilia together with marked ultrastructural abnormalities. Although expression levels of several Aβ-associated transporters, including ABCC1 and LRP1, were largely preserved in APPKI×Ptpn20KO mice, epithelial Aβ accumulation remained markedly increased. Importantly, transcriptomic analyses did not demonstrate major upregulation of App, Bace1, or Bace2 expression in Ptpn20-deficient choroid plexus tissue, suggesting that the observed Aβ accumulation is unlikely to be primarily explained by enhanced amyloid production pathways.

The marked reduction in apical vesicle-like structures observed ultrastructurally further supports the concept that disruption of epithelial architecture extends beyond cytoskeletal abnormalities to include impaired vesicle-associated transport machinery.

These findings suggest that transporter expression alone may be insufficient, as appropriate membrane localization of transporters and preservation of epithelial organization appear equally critical for effective Aβ handling. Our observations further support a model in which cytoskeletal integrity contributes to maintenance of epithelial membrane organization associated with vesicle-associated transport processes.

Importantly, epithelial dysfunction at the level of the ChP was accompanied by accelerated Aβ pathology in the brain parenchyma. APPKI × Ptpn20KO mice exhibited markedly increased cortical and hippocampal plaque deposition, synaptic degeneration, and cognitive impairment compared with APPKI mice alone. These findings provide experimental evidence that primary ChP epithelial dysfunction can accelerate cerebral amyloid pathology. Our findings therefore extend accumulating evidence that alterations in CSF dynamics and barrier-associated epithelial function are linked to the progression of Alzheimer's disease pathology. In line with this interpretation, previous studies have suggested that alterations in cerebrospinal fluid dynamics and barrier-associated transport processes may modulate amyloid pathology and cognitive decline in Alzheimer's disease [30-33].

Beyond its role in solute transport, the ChP is increasingly recognized as an important neuroimmune interface that regulates immune surveillance, cytokine signaling, and communication between the central nervous system and the peripheral immune system[16] [34]. Preservation of epithelial architecture may influence additional functions of the choroid plexus beyond solute transport, including neuroimmune communication, which warrants future investigation.

In addition to the ChP, Aβ clearance from the brain involves multiple pathways, including transport across the blood–brain barrier, perivascular drainage, and glymphatic flow. Unlike the blood–brain barrier, the choroid plexus directly interfaces with the CSF and therefore occupies a distinct position in regulating ventricular solute exchange. The present findings do not exclude contributions of these mechanisms; rather, they suggest that dysfunction of the blood–CSF barrier may represent an additional or complementary component of impaired solute homeostasis. Future studies integrating blood–brain

barrier transport measurements and in vivo clearance assays will be required to clarify the relative contribution of these pathways.

Overall, this work identifies Ptpn20 as a previously unrecognized regulator of ChP epithelial integrity and actin-associated epithelial organization. By maintaining apical F-actin architecture and appropriate RhoA signaling dynamics, Ptpn20 appears to support epithelial membrane organization associated with vesicle-related processes at the blood–CSF barrier. Loss of Ptpn20 was associated with epithelial ultrastructural abnormalities, abnormal Aβ retention at the ventricular-facing apical surface of the ChP epithelium, and accelerated amyloid pathology in vivo. Collectively, our findings support a model in which preservation of epithelial architecture, rather than transporter abundance alone, is essential for effective Aβ handling at the blood–CSF barrier.

Our findings also have potential implications for choroid plexus cauterization, which is used as an adjunctive treatment for hydrocephalus. Preservation of choroid plexus epithelial integrity may be important not only for CSF production but also for maintaining amyloid-β homeostasis. Although surgical injury was not examined in the present study, the long-term consequences of extensive choroid plexus ablation warrant further investigation.

Our findings identify Ptpn20 as a previously unrecognized regulator of choroid plexus epithelial integrity and demonstrate that preservation of epithelial architecture is essential for maintaining amyloid-β homeostasis in Alzheimer's disease.

Limitations and future directions

Several limitations should be considered.

First, although Ptpn20 expression is enriched in the ChP epithelium, low levels are detectable in other central nervous system cell types, including ependymal and glial populations. The relative contributions of these cell types to Aβ handling and barrier-associated epithelial organization remain unresolved. Future studies employing cell-type-specific Ptpn20 deletion will help delineate compartment-specific roles.

Second, while our results support an association between Ptpn20 deficiency and altered RhoA-related actin organization, the direct biochemical substrates and interacting partners of Ptpn20 were not identified. Proteomic and phosphoproteomic approaches will be required to determine whether Ptpn20 acts through direct dephosphorylation of RhoA regulatory pathways or through parallel cytoskeletal mechanisms. The proposed relationships between Ptpn20, RhoA-associated signaling, and epithelial membrane organization should therefore be regarded as a working model requiring further mechanistic validation.

Third, although our findings are consistent with altered Aβ-associated epithelial handling and transport-related processes in Ptpn20-deficient ChP, we did not directly quantify vectorial Aβ movement across the epithelial layer. The present study was designed primarily to examine the consequences of chronic

epithelial dysfunction under progressive amyloid pathology rather than acute tracer kinetics under artificial loading conditions. Future microfluidic, in situ perfusion, or ex vivo barrier assays will be required to evaluate directional Aβ transport dynamics and to further clarify the relative contributions of uptake, intracellular handling, and basolateral efflux.

Finally, the accelerated pathology observed in APPKI × Ptpn20KO mice suggests that preservation of ChP epithelial integrity may represent a potential therapeutic strategy in early AD. Future studies should investigate whether stabilization of actin organization or modulation of RhoA-associated signaling pathways can mitigate epithelial degeneration and Aβ-associated pathology.

Abbreviations

Aβ
Amyloid-beta
Aβ40
Amyloid-beta 1–40
Aβ42
Amyloid-beta 1–42
ABCC1
ATP-binding cassette subfamily C member 1
AD
Alzheimer's disease
ANOVA
Analysis of variance
APP
Amyloid precursor protein
APPKI
APP^{NL-G-F} knock-in mouse
AQP1
Aquaporin-1
ARRIVE
Animal Research:Reporting of In Vivo Experiments
BCA
Bicinchoninic acid
BCSFB
Blood–cerebrospinal fluid barrier
CA3
Cornu Ammonis area 3
Cav1
Caveolin-1

ChP
Choroid plexus
Cltc
Clathrin heavy chain
CNS
Central nervous system
CRISPR
Clustered Regularly Interspaced Short Palindromic Repeats
CSF
Cerebrospinal fluid
DAB
3,3'-Diaminobenzidine
DAPI
4',6-Diamidino-2-phenylindole
DNA
Deoxyribonucleic acid
ELISA
Enzyme-linked immunosorbent assay
F-actin
Filamentous actin
G-LISA
GTPase-linked immunosorbent assay
KI
Knockin
KO
Knockout
LRP1
Low-density lipoprotein receptor-related protein 1
mRNA
Messenger RNA
NIH
National Institutes of Health
PBS
Phosphate-buffered saline
PCR
Polymerase chain reaction
PFA
Paraformaldehyde
PTP
Protein tyrosine phosphatase

Ptpn20
Protein tyrosine phosphatase non-receptor type 20
Ptpn20KO
Ptpn20 knockout
qRT-PCR
Quantitative reverse transcription polymerase chain reaction
RNA
Ribonucleic acid
ROI
Region of interest
RT-PCR
Reverse transcription polymerase chain reaction
RhoA
Ras homolog family member A
SEM
Scanning electron microscopy
SPSS
Statistical Package for the Social Sciences
TEM
Transmission electron microscopy
WT
Wild type

Declarations

Ethics approval and consent to participate:

All animal experiments were reviewed and approved by the Ethics Review Committee for Animal Experimentation of the Juntendo University School of Medicine (approval number 1337). All procedures complied with institutional guidelines, national regulations, and the National Institutes of Health (NIH) Guide for the Care and Use of Laboratory Animals. The study was designed, conducted, and reported in accordance with the ARRIVE 2.0 guidelines. Animals were housed under controlled temperature and humidity conditions with a 12-hour light/dark cycle and monitored daily for health and well-being. All efforts were made to minimize animal suffering and to reduce the number of animals used.

Clinical trial number: not applicable.

Consent for publication:

Not applicable

Availability of data and materials:

The datasets generated and/or analyzed during the current study are available from the corresponding author on reasonable request.

Competing interests:

The authors declare that they have no competing interests.

Funding:

This work was supported by the Juntendo Research Branding Project and the Japan Society for the Promotion of Science (JSPS) KAKENHI (Grant Numbers 23K15674 and 24K10497). The funding bodies had no role in the study design, data collection, data analysis, interpretation of the data, or writing of the manuscript.

Authors' contributions:

M.M.: Conceptualization, Supervision, Funding Acquisition, Writing – Review & Editing.

R.M.: Investigation, Formal Analysis, Data Curation, Visualization, Writing – Original Draft.

M.N. and A.K.: Methodology, Investigation.

S.Y., K.K., C.A., K.S., K.H., and C.K.: Investigation, Data Curation.

I.O.: Investigation.

E.N. and N.T.: Resources, Methodology.

All authors reviewed and approved the final manuscript.

Acknowledgements:

We thank Dr. Takeomi C. Saido (Laboratory for Proteolytic Neuroscience, RIKEN Center for Brain Science) and Dr. Takashi Saito (Department of Neurocognitive Science, Institute of Brain Science, Nagoya City University) for generously providing the APP^NL-G-F knock-in mice used in this study. We also thank the Laboratory of Proteomics and Biomolecular Science, the Laboratory of Molecular and Biochemical Research, the Laboratory of Morphology and Image Analysis, the Laboratory of Biomedical Research Resources, the Research Support Centre, the Graduate School Research Program of Juntendo University, the Juntendo University Research Institute for Diseases of Old Age, and the Juntendo University Graduate School of Medicine for technical assistance.

References

1. Zhang J, Zhang Y, Wang J, Xia Y, Zhang J, Chen L (2024) Recent advances in Alzheimer's disease: mechanisms, clinical trials and new drug development strategies. Signal Transduct Target Therapy

9(1):211

2. Morató X, Pytel V, Jofresa S, Ruiz A, Boada M (2022) Symptomatic and Disease-Modifying Therapy Pipeline for Alzheimer's Disease: Towards a Personalized Polypharmacology Patient-Centered Approach. Int J Mol Sci 23(16):9305
3. Aisen PS, Cummings J, Jack CR, Morris JC, Sperling R, Frölich L et al (2017) On the path to 2025: understanding the Alzheimer's disease continuum. Alzheimers Res Ther 9(1):60
4. Behl C (2024) In. the amyloid-cascade-hypothesis still remains a working hypothesis, no less but certainly no more. Front Aging Neurosci. 2024;16:1459224
5. Fontana IC, Zimmer AR, Rocha AS, Gosmann G, Souza DO, Lourenco MV et al (2020) Amyloid-beta oligomers in cellular models of Alzheimer's disease. J Neurochem 155(4):348–369
6. Kepp KP, Robakis NK, Hoilund-Carlsen PF, Sensi SL, Vissel B (2023) The amyloid cascade hypothesis: an updated critical review. Brain 146(10):3969–3990
7. Gião T, Teixeira T, Almeida MR, Cardoso I (2022) Choroid Plexus in Alzheimer's Disease—The Current State of Knowledge. Biomedicines 10(2):224
8. Balusu S, Brkic M, Libert C, Vandenbroucke RE (2016) The choroid plexus-cerebrospinal fluid interface in Alzheimer's disease: more than just a barrier. Neural Regeneration Res 11(4):534–537
9. Matsumoto K, Chiba Y, Fujihara R, Kubo H, Sakamoto H, Ueno M (2015) Immunohistochemical analysis of transporters related to clearance of amyloid-beta peptides through blood-cerebrospinal fluid barrier in human brain. Histochem Cell Biol 144(6):597–611
10. Delvenne A, Vandendriessche C, Gobom J, Burgelman M, Dujardin P, De Nolf C et al (2024) Involvement of the choroid plexus in Alzheimer's disease pathophysiology: findings from mouse and human proteomic studies. Fluids Barriers CNS 21(1):58
11. Municio C, Carrero L, Antequera D, Carro E (2023) Choroid Plexus Aquaporins in CSF Homeostasis and the Glymphatic System: Their Relevance for Alzheimer's Disease. Int J Mol Sci. ;24(1)
12. Saunders NR, Dziegielewska KM, Fame RM, Lehtinen MK, Liddelow SA (2023) The choroid plexus: a missing link in our understanding of brain development and function. Physiol Rev 103(1):919–956
13. Tietz S, Engelhardt B (2015) Brain barriers: Crosstalk between complex tight junctions and adherens junctions. J Cell Biol 209(4):493–506
14. Baehr C, Reichel V, Fricker G (2006) Choroid plexus epithelial monolayers – a cell culture model from porcine brain. Cerebrospinal Fluid Res 3(1):13
15. Sadanandan J, Sathyanesan M, Newton SS (2024) Aging alters the expression of trophic factors and tight junction proteins in the mouse choroid plexus. Fluids Barriers CNS 21(1):77
16. Dani N, Herbst RH, McCabe C, Green GS, Kaiser K, Head JP et al (2021) A cellular and spatial map of the choroid plexus across brain ventricles and ages. Cell 184(11):3056–74e21
17. Scarpetta V, Bodaleo F, Salio C, Agarwal A, Sassoe-Pognetto M, Patrizi A (2023) Morphological and mitochondrial changes in murine choroid plexus epithelial cells during healthy aging. Fluids Barriers CNS 20(1):19

18. Eide PK, Pripp AH, Ringstad G (2020) Magnetic resonance imaging biomarkers of cerebrospinal fluid tracer dynamics in idiopathic normal pressure hydrocephalus. Brain Commun. ;2(2)
19. Murakami Y, Matsumoto Y, Hoshi K, Ito H, Fuwa TJ, Yamaguchi Y et al (2018) Rapid increase of 'brain-type' transferrin in cerebrospinal fluid after shunt surgery for idiopathic normal pressure hydrocephalus: a prognosis marker for cognitive recovery. J Biochem 164(3):205–213
20. Murakami Y, Saito K, Ito H, Hashimoto Y (2019) Transferrin isoforms in cerebrospinal fluid and their relation to neurological diseases. Proc Jpn Acad Ser B Phys Biol Sci 95(5):198–210
21. Silverberg GD, Levinthal E, Sullivan EV, Bloch DA, Chang SD, Leverenz J et al (2002) Assessment of low-flow CSF drainage as a treatment for AD. Neurology 59(8):1139–1145
22. Xu H, Miyajima M, Nakajima M, Ogino I, Kawamura K, Akiba C et al (2022) Ptpn20 deletion in H-Tx rats enhances phosphorylation of the NKCC1 cotransporter in the choroid plexus: an evidence of genetic risk for hydrocephalus in an experimental study. Fluids Barriers CNS 19(1):39
23. Fodero-Tavoletti MT, Hardy MP, Cornell B, Katsis F, Sadek CM, Mitchell CA et al (2005) Protein tyrosine phosphatase hPTPN20a is targeted to sites of actin polymerization. Biochem J 389(Pt 2):343–354
24. Young KA, Biggins L, Sharpe HJ (2021) Protein tyrosine phosphatases in cell adhesion. Biochem J 478(5):1061–1083
25. Zuo X, Zhao X, Zhang X, Li Q, Jiang X, Huang S et al (2024) PTPN20 promotes metastasis through activating NF-κB signaling in triple-negative breast cancer. Breast Cancer Res 26(1):155
26. Saito T, Matsuba Y, Mihira N, Takano J, Nilsson P, Itohara S et al (2014) Single App knock-in mouse models of Alzheimer's disease. Nat Neurosci 17(5):661–663
27. Ridley AJ, Hall A (1992) The small GTP-binding protein rho regulates the assembly of focal adhesions and actin stress fibers in response to growth factors. Cell 70(3):389–399
28. Amano M, Nakayama M, Kaibuchi K (2010) Rho-kinase/ROCK: A key regulator of the cytoskeleton and cell polarity. Cytoskeleton (Hoboken) 67(9):545–554
29. Nishimura Y, Yoshioka K, Bernard O, Bereczky B, Itoh K (2006) A role of LIM kinase 1/cofilin pathway in regulating endocytic trafficking of EGF receptor in human breast cancer cells. Histochem Cell Biol 126(5):627–638
30. Brkic M, Balusu S, Van Wonterghem E, Gorle N, Benilova I, Kremer A et al (2015) Amyloid beta Oligomers Disrupt Blood-CSF Barrier Integrity by Activating Matrix Metalloproteinases. J Neurosci 35(37):12766–12778
31. Silverberg GD, Heit G, Huhn S, Jaffe RA, Chang SD, Bronte–Stewart H et al (2001) The cerebrospinal fluid production rate is reduced in dementia of the Alzheimer’s type. Neurology 57(10):1763–1766
32. González-Marrero I, Giménez-Llort L, Johanson CE, Carmona-Calero EM, Castañeyra-Ruiz L, Brito-Armas JM et al (2015) Choroid plexus dysfunction impairs beta-amyloid clearance in a triple transgenic mouse model of Alzheimer's disease. Front Cell Neurosci 9:17

33. Kant S, Stopa EG, Johanson CE, Baird A, Silverberg GD (2018) Choroid plexus genes for CSF production and brain homeostasis are altered in Alzheimer's disease. Fluids Barriers CNS 15(1):34
34. Saunders NR, Dziegielewska KM, Fame RM, Lehtinen MK, Liddelow SA (2023) The choroid plexus: a missing link in our understanding of brain development and function. Physiol Rev 103(1):919–956

Tables

Table 1

Primer sequences and PCR product sizes for genotyping

Gene (Allele)	Primer Direction	Sequence (5'→3')	PCR Product Size
APP^NL-G-F	Forward	CTCCTTGTGGCTGGCGGTCACAC	670 bp (WT) / 870 bp (Mutant)
	Reverse	CTATCGTGGACCGAGAATGGTCATG	—
Ptpn20 (KO allele)	Forward	TCATGGACACTGAAATACAGG	505 bp (WT) / 410 bp (KO)
	Reverse	AATAGCGTCAATGGTCTAAGAG	—

Table 2

Assay IDs of Real-time PCR

Target	TaqMan Assay ID
Ptpn20	Ptpn20, Mm00477234_m1
Cav1	Cav1, Mm00483057_m1
Cltc	Cltc, Mm01303974_m1
Lrp1	Lrp1, Mm00464608_m1
Abcc1	Abcc1, Mm00456156_m1
AQP1	AQP1, Mm00431834_m1
Na^+, K^+-ATPase	ATP1a1, Mm00523255_m1
Slc13a3	Slc13a3, Mm00475289m1
Actin	Actb, Mm00607939_S1

Table 3

Reagents for immunofluorescence investigations

Fig No	Method	Target	Reagents	
			Primary antibody	Secondary antibody
1-a	Cryosection	Ptpn20	Rabbit PTPN20B antibody (CSB-PA065165, CusAb, 1:250)	Donkey anti-Rabbit IgG (H + L) Alexa Fluor™ Plus 488 (A32790, Invitrogen, 1:25)
1-e, f	Cryosection	RhoA	Mouse RhoA antibody 66733-1-IG (Proteintech Group.Inc.,1:100)	Donkey anti-Mouse IgG (H + L) Alexa Fluor™ Plus 488 (A32766, Invitrogen, 1:25)
1-c	Free-floating	AQP1	Mouse AQP1- antibody (B-11) sc-25287 (Santa Cruz Biotechnology, 1:25)	Donkey anti-Mouse IgG (H + L) Alexa Fluor™ Plus 488 (A32766, Invitrogen, 1:25)
1-a, e, f	Cryosection	F-Actin	Actin-stain 555 Fluorescent Phalloidin (Cat. # PHDH1, Cytoskeleton. Inc., 1:50)	
3-a	FFPE	Amyloid	Anti-Human Amyloidβ (N) (82E1) Mouse IgG MoAb #10323 (Immuno-Biological Laboratories Co., Ltd 1:100)	Donkey anti-Mouse IgG (H + L) Alexa Fluor™ Plus 488 (A32766, Invitrogen, 1:25)
3-c	Free-floating	LRP1	Rabbit LRP1- antibody (EPR3724) AB92544 (Abcam, 1:50)	Donkey anti-Rabbit IgG (H + L) Alexa Fluor™ Plus 488 (A32790, Invitrogen, 1:50)
3-c	Free-floating	Amyloid	Anti-Human Amyloidβ (N) (82E1) Mouse IgG MoAb #10323 (Immuno-Biological Laboratories Co., Ltd 1:50)	Donkey anti-Mouse IgG (H + L) Alexa Fluor™ Plus 594 (A32744, Invitrogen, 1:50)

Table 4

Reagents for immunohistochemistry

Fig No	Method	Target	Reagents	
			Treatment / Condition	Primary antibody
2-d	Paraffin	Claudin	Antigen Unmasking Solution,Citric Acid Based (VECTOR LABORATORIES, 1:100) 121℃ 10min	Rabbit Claudin1 antibody 28674-1-AP(Proteintech Group.Inc.,1:500)
5-a, c	Paraffin	Amyloid	Formic acid 11-0780-5 (SIGMAALDRICH) 5min	Anti-Human Amyloidβ (N) (82E1) Mouse IgG MoAb #10323 (IBL 1:100)

Figures

Fig.1

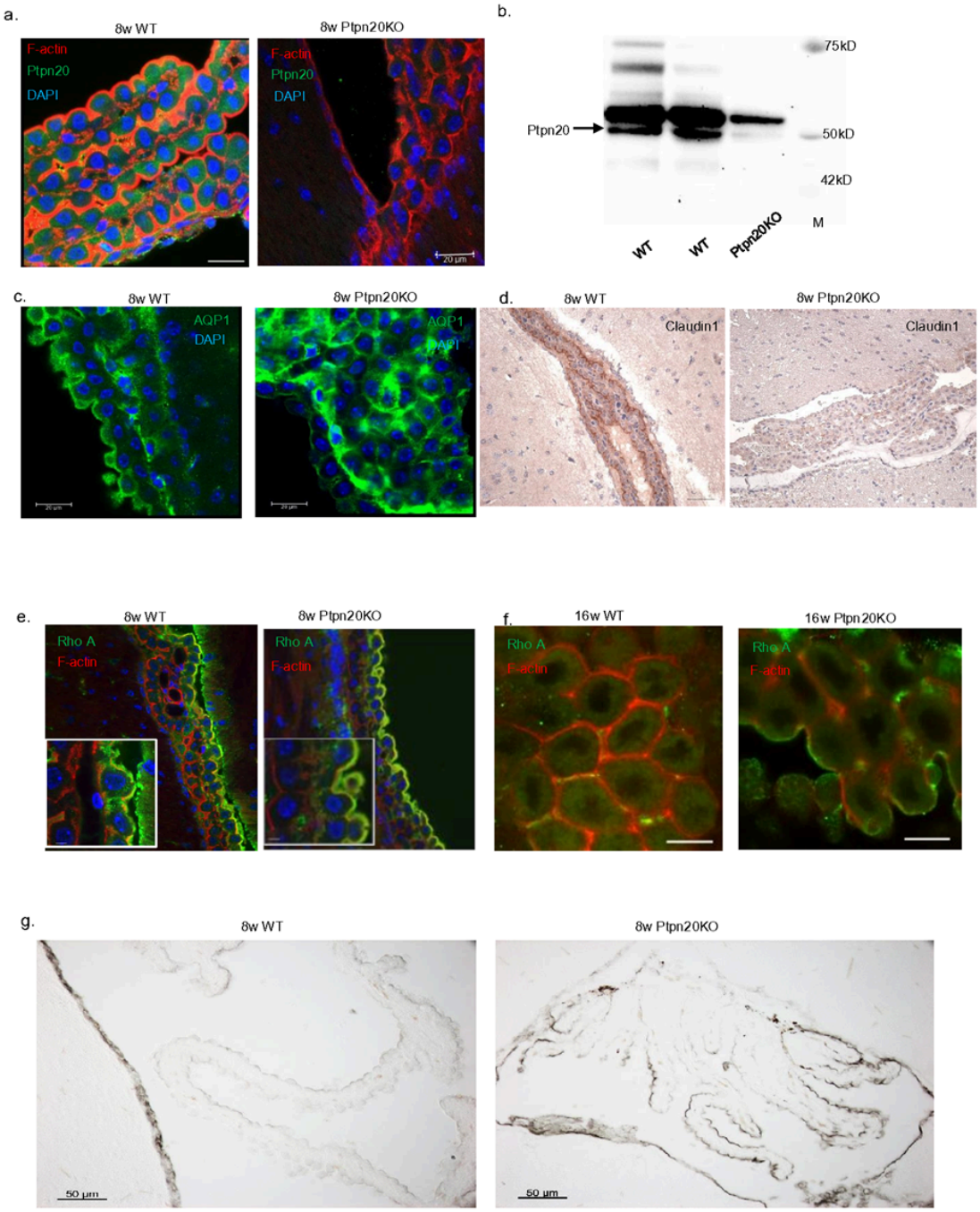


Figure 1

Ptpn20 deficiency disrupts choroid plexus (ChP) epithelial integrity

a, Immunofluorescence staining of Ptpn20 (green) and F-actin (red) in WT and Ptpn20KO mice at 8

weeks of age. Ptpn20 immunoreactivity is absent in Ptpn20KO mice, accompanied by marked disruption and thinning of apical F-actin organization. Scale bars = 20 μm.

b, Western blot analysis confirming loss of Ptpn20 protein expression in ChP tissue from Ptpn20KO mice.

c, Immunofluorescence staining for AQP1 (green); WT ChP epithelium shows predominantly apical membrane-associated AQP1 staining, whereas Ptpn20KO mice exhibit a less continuous and irregular AQP1 pattern with partial cytoplasmic redistribution. Nuclei are counterstained with DAPI. Scale bars = 20 μm.

d, Immunostaining for claudin-1 demonstrates reduced claudin-1 immunoreactivity along the epithelial junctions in Ptpn20KO ChP epithelium compared with WT controls. Representative images are shown. Scale bars = 50 μm.

e, Immunofluorescence staining for RhoA (green) and F-actin (red) shows apical localization of RhoA in both WT and Ptpn20KO ChP epithelium at 8 weeks of age. Scale bars = 20 μm.

f, WT mice show preserved apical F-actin organization and apical epithelial architecture, whereas Ptpn20KO mice exhibit severe disruption of apical F-actin organization. Scale bars = 5 μm.
g, Intracisternal Carbon Black 30 min after injection reveals minimal epithelial tracer retention in WT ChP epithelium, whereas Ptpn20KO mice exhibit marked apical tracer retention. Scale bars = 50 μm.

Fig.2

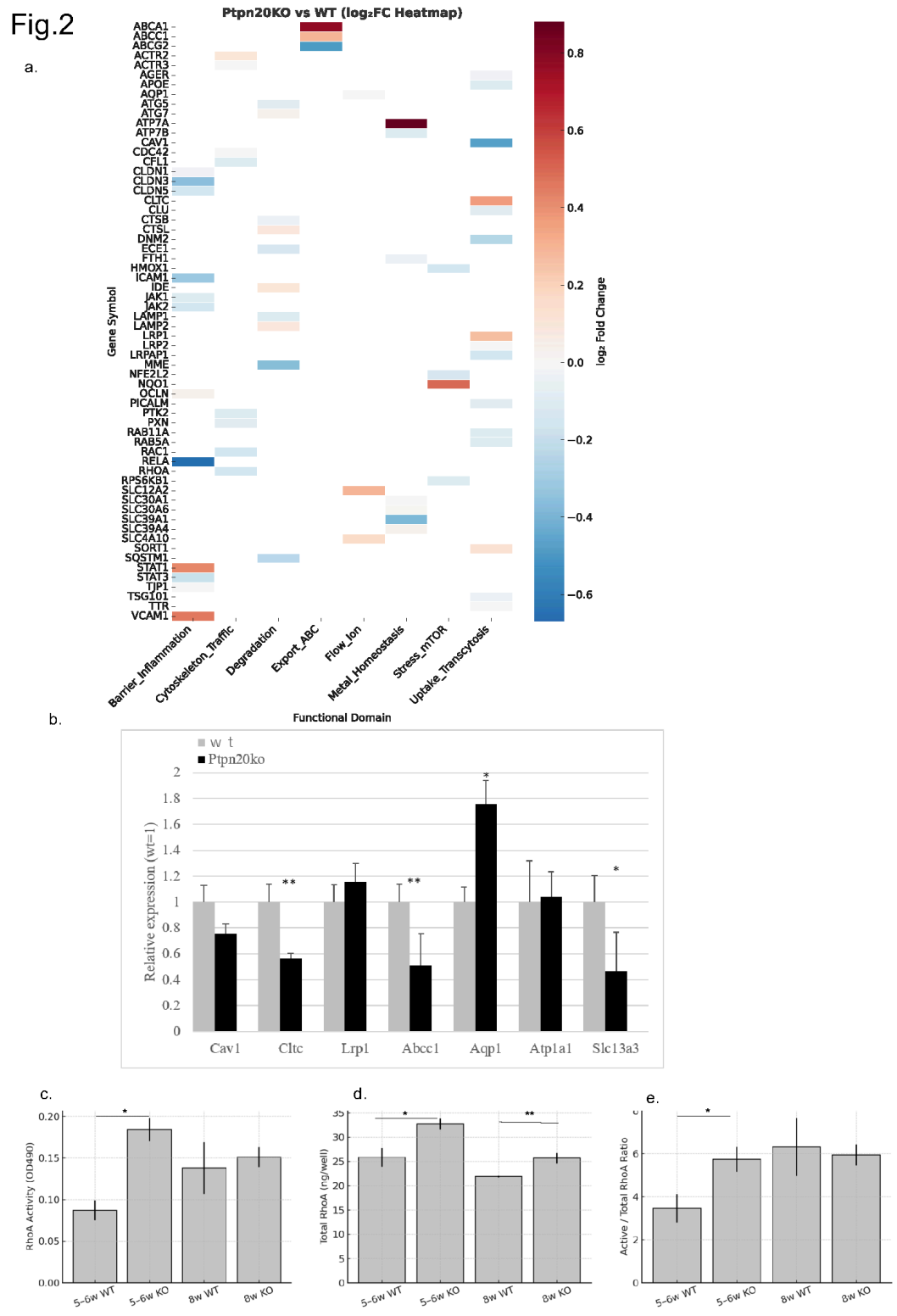


Figure 2

Ptpn20 deficiency alters epithelial transport-related pathways and RhoA signaling

a, Heat map showing relative gene expression changes identified by transcriptomic profiling of choroid plexus tissue from 4-week-old Ptpn20KO mice compared with WT controls. Genes were grouped into eight functional categories: barrier/inflammation, cytoskeleton/vesicle-associated transport

organization, degradation, export/ABC transporters, flow ion transport, metal homeostasis, stress/mTOR signaling, and uptake/transcytosis. Color intensity represents $\log_2$ fold-change values, with red indicating increased expression and blue indicating decreased expression in Ptpn20KO mice relative to WT controls.

b, RT–qPCR validation of selected genes involved in epithelial transport and barrier function in 5-week-old ChP. Gene expression levels were normalized to WT controls (WT = 1). Cav1, Cltc, Abcc1, and Aqp1 expression levels were significantly reduced in Ptpn20KO mice, whereas Lrp1, Atp1a1 and Slc13a3 show no significant changes. Analyses were performed using ChP tissue from 5-week-old mice (WT: n=5, Ptpn20KO: n=4). Data are presented as mean ± s.e.m. Statistical analysis was performed using two-tailed unpaired Student's *t*-tests.

c, Quantification of active, GTP-bound RhoA using a G-LISA assay. At 5–6 weeks, Ptpn20KO mice show significantly elevated active RhoA levels compared with WT controls, whereas no significant difference is observed at 8 weeks.
d, Total RhoA protein levels measured by ELISA. Ptpn20KO mice exhibit modest but significant increases at both 5–6 weeks and 8 weeks.
e, Ratio of active to total RhoA, representing the fraction of GTP-bound RhoA. The ratio is significantly elevated in Ptpn20KO mice at 5–6 weeks but returns toward WT levels by 8 weeks. **Active and total RhoA levels were measured in the same mice (5–6 weeks: WT n=3, Ptpn20KO n=8; 8 weeks: WT n=3, Ptpn20KO n=7).** Data in **c–e** are presented as mean ± s.e.m. Statistical significance was assessed using two-tailed unpaired Student's *t*-tests.

Fig.3

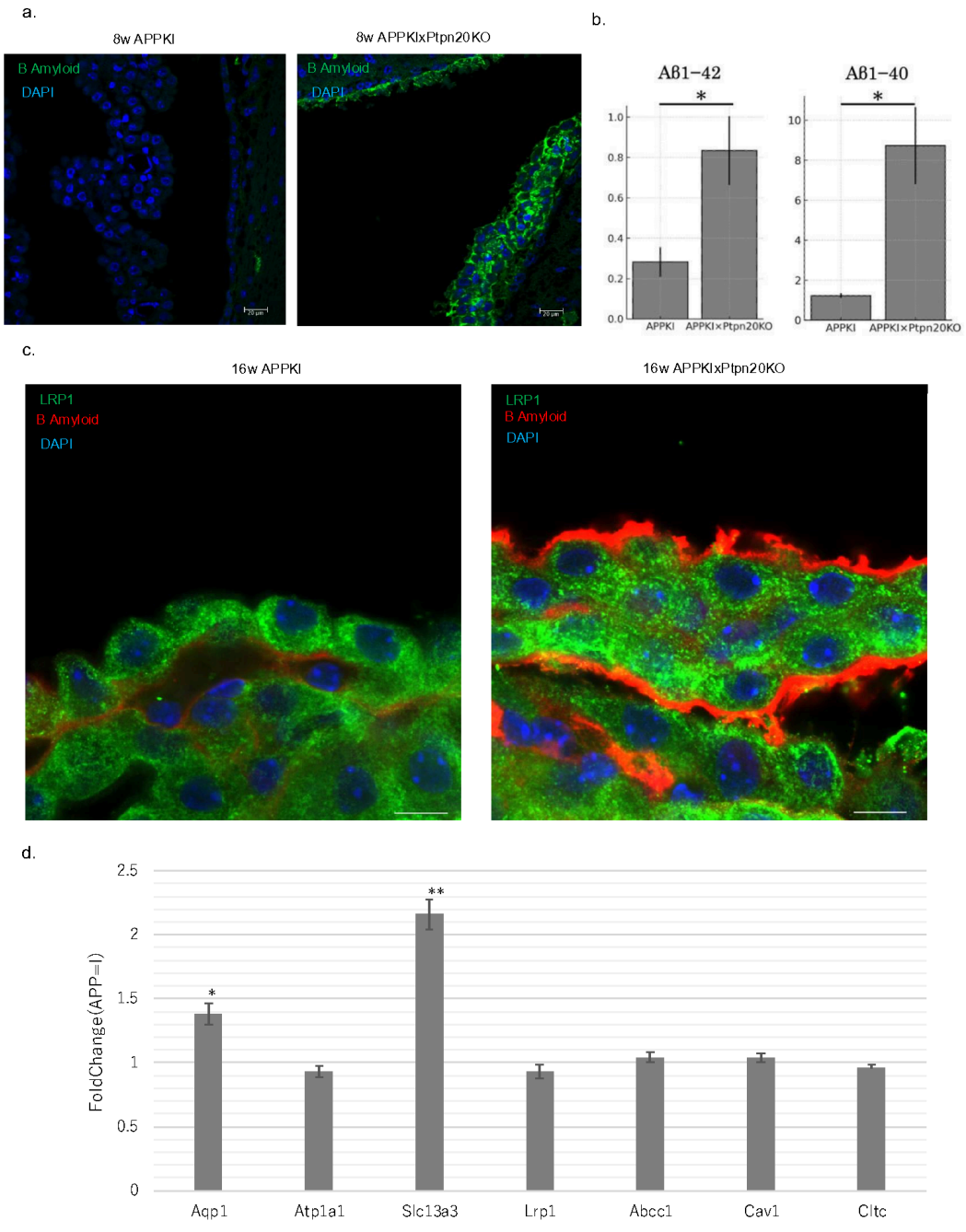


Figure 3

Choroid plexus (ChP) epithelial dysfunction promotes ventricular-facing Aβ retention in APPKI mice

a, Representative immunofluorescence staining for Aβ (green) in the ChP of APPKI and APPKI×Ptpn20KO mice. APPKI×Ptpn20KO mice exhibit marked retention of Aβ along the ventricular-facing surface of the ChP epithelium compared with APPKI mice. Nuclei are counterstained with DAPI

(blue). Scale bars = 20 μm.
b, ELISA quantification of Aβ40 and Aβ42 in ChP tissue lysates at 8 weeks of age. Both Aβ species are significantly elevated in APPKI × Ptpn20KO mice compared with APPKI controls. Aβ40 and Aβ42 levels were measured in the same mice (APPKI: n=4, APPKI × Ptpn20KO: n=5). Data are presented as mean ± s.e.m. Statistical significance was determined using two-tailed unpaired Student's *t*-tests.

c, Double immunofluorescence staining for LRP1 (green) and amyloid-β (red) in the choroid plexus of APPKI and APPKI×Ptpn20KO mice. At 16 weeks of age, APPKI mice showed mild amyloid-β immunoreactivity predominantly within the stromal region, whereas APPKI×Ptpn20KO mice exhibited prominent amyloid-β deposition along the ventricular-facing epithelial surface. LRP1 immunoreactivity was broadly distributed throughout the choroid plexus epithelium in both genotypes. Nuclei were counterstained with DAPI. Scale bars = 5 μm.

d, RT–qPCR analysis of selected epithelial transport- and membrane-associated genes in choroid plexus tissue from 7-week-old APPKI and APPKI×Ptpn20KO mice. Gene expression levels were normalized to APPKI controls (APPKI = 1). APPKI×Ptpn20KO mice exhibited increased Aqp1 and Slc13a3 expression, whereas Lrp1, Atp1a1, Abcc1, Cav1, and Cltc expression remained largely unchanged. Data are presented as mean ± s.e.m. Analyses were performed using choroid plexus tissue from APPKI (n = 5) and APPKI×Ptpn20KO (n = 5) mice. Statistical significance was assessed using two-tailed unpaired Student's t-tests.

Fig.4

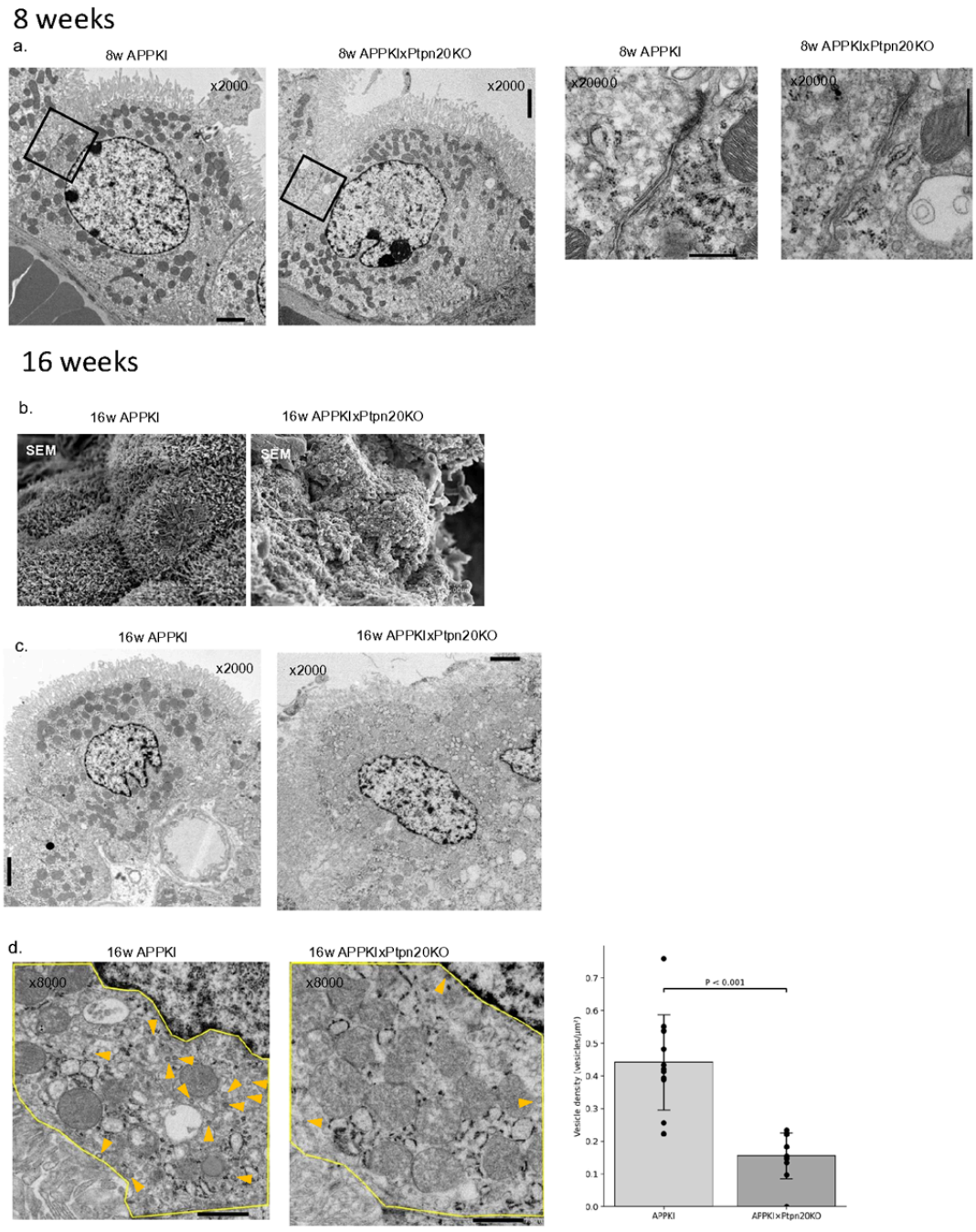


Figure 4

Loss of epithelial ultrastructure and apical vesicle organization in APPKI × Ptpn20KO mice

a, TEM images of the choroid plexus epithelium at 8 weeks of age. APPKI×Ptpn20KO mice exhibit abnormalities at the apical junctional region together with enlargement of intercellular spaces compared with APPKI controls. Scale bars = 2 µm (x2000), 500 nm (x20000) and 1 µm (x5000).

b, c, Representative SEM and TEM images at 16 weeks of age demonstrating progressive epithelial degeneration in APPKI×Ptpn20KO mice, including disruption of the apical epithelial surface, altered cytoplasmic organization, marked loss of apical microvilli and cilia, and abnormal mitochondrial profiles. SEM; Scale bars = 1 μm (×8000), TEM; Scale bars = 1 μm (x7000).

d, Quantification of apical vesicle-like structures per unit apical epithelial area demonstrated a significant reduction in APPKI × Ptpn20KO mice compared with APPKI controls. Vesicle-like structures measuring 50–150 nm in diameter and located within 2 μm of the apical membrane were quantified in a blinded manner. Each dot represents one animal (APPKI: n = 10, APPKI × Ptpn20KO: n = 10). Data are presented as mean ± s.d. Statistical significance was determined using a two-tailed unpaired Student's t-test ($P < 0.001$).

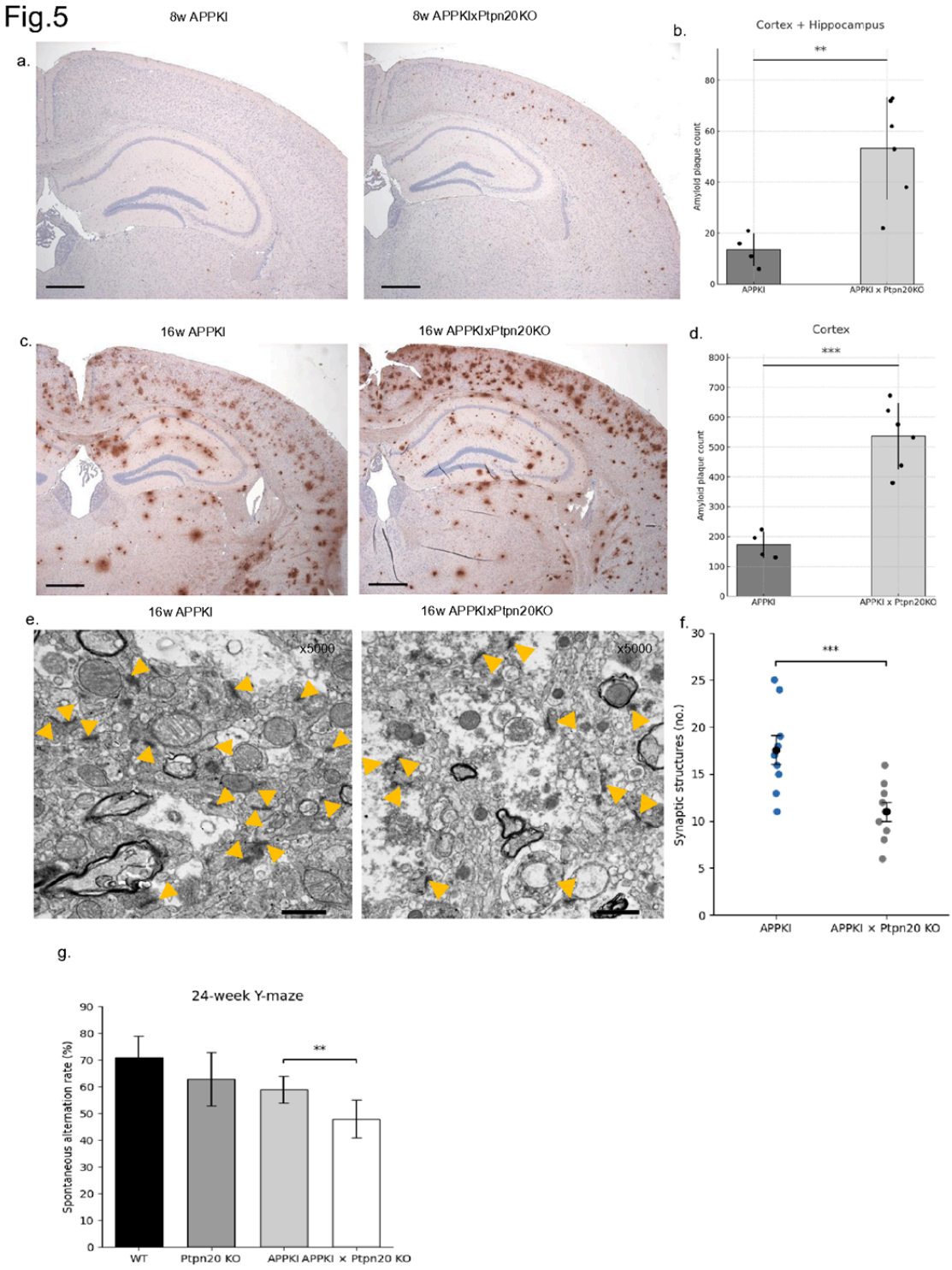


Figure 5

Choroid plexus dysfunction accelerates brain amyloid pathology and cognitive decline

a, Immunohistochemical detection of amyloid plaques in the cerebral cortex and hippocampus at 8 weeks of age. APPKI × Ptpn20KO mice exhibited markedly increased plaque burden in the cerebral

cortex and hippocampus compared with APPKI mice. Scale bars = 500 μm.
b, Quantification of cortical and hippocampal plaque burden at 8 weeks.

c, Representative immunohistochemical images showing increased amyloid plaque accumulation in the cortex and hippocampus at 16 weeks of age. Scale bars = 500 μm.
d, Quantification of cortical plaque burden at 16 weeks demonstrated significantly greater plaque accumulation in APPKI × Ptpn20KO mice compared with APPKI controls. Data in **b** and **d** are presented as mean ± s.d. Analyses were performed using cortex and hippocampal sections from APPKI (n=4) and APPKI × Ptpn20KO (n=5) mice. Statistical analysis was performed using two-tailed unpaired Student's *t*-tests.

e, Representative TEM images of the hippocampal CA3 region from 16-week-old APPKI and APPKI × Ptpn20KO mice. APPKI × Ptpn20KO mice exhibited a marked reduction of synaptic structures compared with APPKI controls.

f. Quantification of density of synaptic structures in the hippocampal CA3 region. Each dot represents one animal (APPKI: n = 9, APPKI × Ptpn20KO: n = 8). Data are presented as mean ± s.d. Statistical significance was determined using a two-tailed unpaired Student's t-test.

g, Spontaneous alternation performance in the Y-maze at 24 weeks of age. APPKI × Ptpn20KO mice showed a significant reduction in alternation rate compared with APPKI mice, indicating impaired working memory. Behavioral analyses were performed using the same cohort of mice (WT: n=6, Ptpn20KO: n=8, APPKI: n=7, APPKI × Ptpn20KO: n=10). Data are presented as mean ± s.e.m. Statistical analysis was performed using one-way ANOVA followed by Tukey's post hoc test.

Fig.6

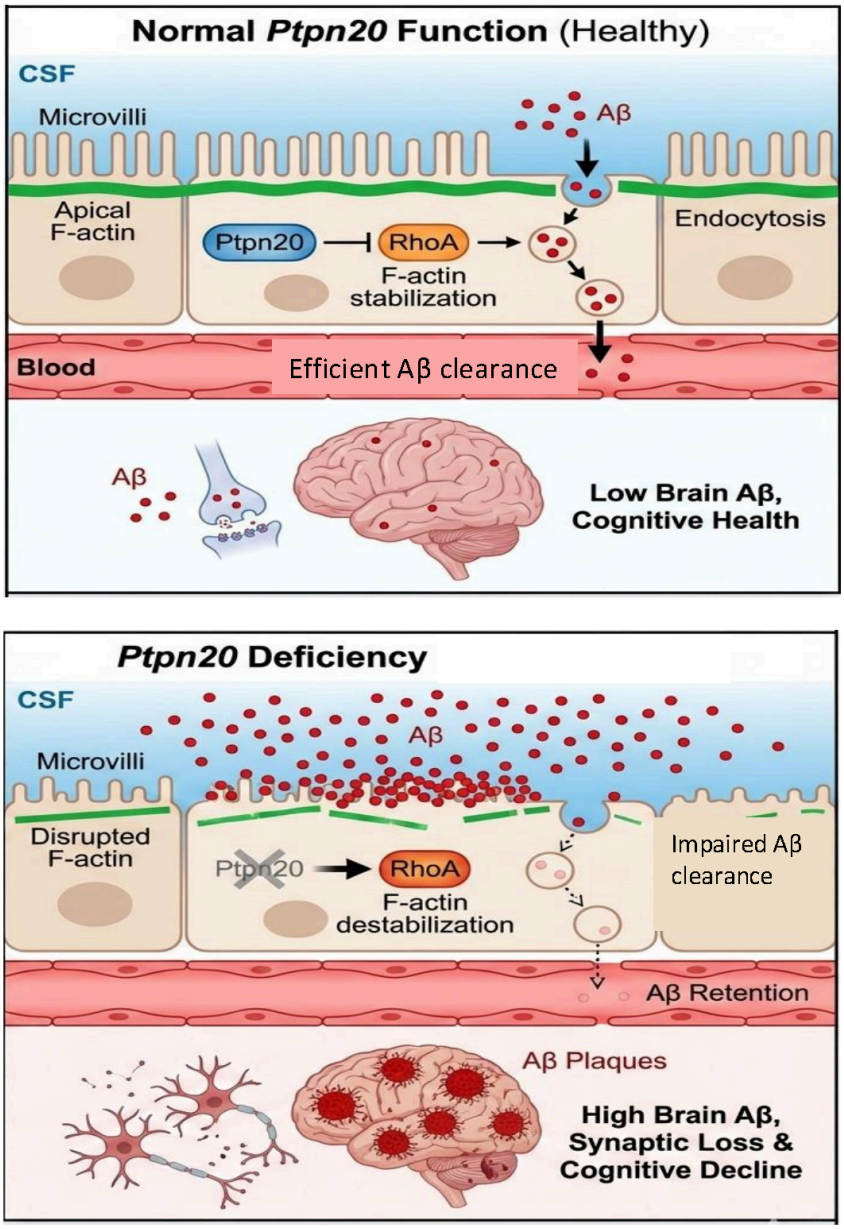


Figure 6

Proposed model.

Proposed model summarizing findings from transcriptomic, ultrastructural, biochemical, and functional analyses. Loss of Ptpn20 disrupts apical F-actin organization and epithelial membrane architecture in the choroid plexus, accompanied by alterations in epithelial transport- and vesicle-associated pathways.

These changes are associated with abnormal amyloid-β retention at the ventricular-facing apical surface of the choroid plexus epithelium and disruption of apical vesicle organization. Collectively, these alterations are proposed to contribute to accelerated cerebral amyloid deposition, synaptic loss, and cognitive impairment in APPKI×Ptpn20KO mice.

Supplementary Files

This is a list of supplementary files associated with this preprint. Click to download.

- SpFigure.pdf
- supplementfileGGel.pdf